

Superconductivity in the vicinity of charge ordered state in organic conductor β -(meso-DMBEDT-TTF)₂PF₆

Kazuyoshi YOSHIMI¹ *, Masaaki NAKAMURA² and Hatsumi MORI¹

¹*Institute for Solid State Physics, University of Tokyo, Kashiwanoha, Kashiwa, Chiba 277-8581*

²*Department of Applied Physics, Faculty of Science, Tokyo University of Science, Kagurazaka, Shinjuku-ku, Tokyo 162-8601*

We study theoretically competition between the charge ordering and the superconductivity in two-dimensional organic conductor β -(meso-DMBEDT-TTF)₂PF₆. We analyze the extended Hubbard model on a weakly-dimerized lattice based on the random phase approximation and Eliashberg equations. We found reentrant behavior of the checkerboard-type charge-ordered phase in the phase diagram, and the triplet superconductivity due to the charge fluctuation in the neighboring region. In the low temperature and high pressure region, the singlet superconductivity also appears due to the enhancement of the spin fluctuation.

KEYWORDS: organic conductor, β -(meso-DMBEDT-TTF)₂PF₆, superconductivity, charge ordering, random phase approximation, Eliashberg equation, charge fluctuation

1. Introduction

Organic conductors have attracted attention for many years. About two decades ago, a superconductivity was found in a low dimensional organic conductor (TMTSF)₂PF₆ at the critical temperature $T_c \approx 0.9$ K under the pressure $p \approx 12$ kbar. Since then, about 130 kinds of organic superconductors have been discovered. It is notable that BEDT-TTF salts (ET salts) are about 50 kinds of them.^{1,2} The ET salts are mainly quasi-two-dimensional (2D) conductors with 3/4-filled π band of the donor molecules. These materials exhibit very interesting electronic properties such as superconductivity, magnetism and charge ordering.

For example, κ -(ET)₂X salts show superconducting (SC) transitions next to the antiferromagnetism in the (p, T) phase diagram. The theoretical calculations based on the half-filled extended Hubbard model where the strong dimerization is assumed show that this superconductivity is mediated by antiferromagnetic spin fluctuations.³⁻⁶ In α -(ET)₂I₃ salt, there are several theoretical works for the superconductivity in the presence of a charge ordering by the random phase approximation (RPA).^{7,8} In this case the SC state is also considered mediated by the antiferromagnetic spin fluctuation. For θ -(ET)₂X salts where the various charge-ordered (CO) states are observed, there are several theoretical works on the CO states by the mean field theory.^{9,10} The superconductivity of this material is explained that it is induced by both the spin and the charge fluctuations.¹¹

In this paper, we focus on β -(meso-DMBEDT-TTF)₂PF₆ salt (β -(DMeET)₂PF₆ salt) which is recently synthesized and investigated by Kimura and Mori *et al.*¹²⁻¹⁴ The conduction layer of this material consists of weakly dimerized two molecules per unit cell with 3/4-filled band, and shows the metal-insulator (MI) transition at $T_{MI} \approx 90$ K, whereas the magnetic susceptibility shows no anomaly around T_{MI} . The insulating state exhibits the checkerboard-type charge order-

ing (see Fig.1(b)) where the charge disproportion occurs within the dimer unit. Estimating the nearest neighbor Coulomb interaction by the point charge approximation, it is reported that the checkerboard type charge ordering does not occur, and the effective molecule size and the electron-phonon interaction should be taken into account.¹² The most remarkable point is that β -(DMeET)₂PF₆ displays a SC state next to the CO state in the (p, T) phase diagram, with the critical temperature $T_c \approx 4$ K under the pressure $p \approx 4$ kbar.^{13,14} T_c decreases with increasing the magnetic field, and the superconducting transition is completely suppressed above 4 T down to 0.5 K.

It is well known that SC transitions often appear next to the magnetic ordered regions of the (p, T) phase diagrams not only in organics but also in heavy fermion systems.¹⁵⁻¹⁷ This has been considered as a typical character of superconductivity with magnetically mediated pairing mechanism. Therefore, the fact that the superconductivity appeared in the neighbor of the CO region is not only new for the organic conductors, but also important for possibilities of the superconductivity due to charge fluctuation. Recently, a superconductivity appearing in the neighboring region of the phase diagram is also found in β -vanadium bronze,¹⁸ but no theoretical studies focused on this material have been done.

From the above background, we study β -(DMeET)₂PF₆ in the following two point of views: i) How the checkerboard-type charge ordering is stabilized in the weakly dimerized organic systems. ii) How the SC region appears in the neighbor of the CO region from the metallic state.

The rest of this paper is organized as follows. In Sec. 2, we formulate susceptibilities and Eliashberg equations based on the RPA for the weakly dimerized 2D system. In Sec. 3, we determine appropriate parameter set of the model, and present results of the numerical analysis. Finally, summary and discussion are given in Sec. 4.

*E-mail address: yoshimi@issp.u-tokyo.ac.jp

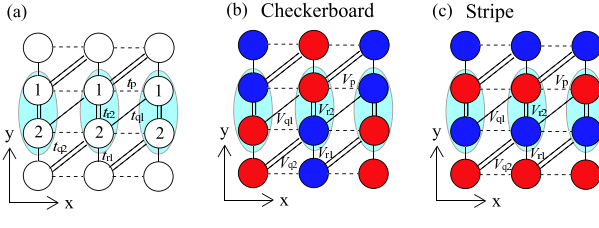


Fig. 1. (a) Model for the conduction layer of β -(DMeET)₂PF₆ salt. The unit cell consists of two molecules labeled 1,2 with transfer integrals: t_{r1} , t_{r2} , t_{q1} , t_{q2} , t_p . We also introduce corresponding nearest neighbor interactions: V_{r1} , V_{r2} , V_{q1} , V_{q2} , V_p . (b),(c) Two candidates of the charge ordered states in the present analysis, the checkerboard type and the stripe type, respectively.

2. Formulation

In this section, we perform the analysis for the Hubbard-type model based on the random phase approximation following Kobayashi *et al.*^{7,8} Throughout this paper we set $k_B = \hbar = 1$.

2.1 Model

We consider the extended Hubbard model on the two-dimensional (2D) lattice (see Fig. 1 (a)),

$$\mathcal{H} = \mathcal{H}_t + \mathcal{H}_U + \mathcal{H}_V, \quad (1)$$

$$\mathcal{H}_t = \sum_{\langle i\alpha; j\beta \rangle} \sum_{\sigma} (t_{i\alpha; j\beta} c_{i\alpha\sigma}^\dagger c_{j\beta\sigma} + \text{H.c.}), \quad (2)$$

$$\mathcal{H}_U = \sum_{i\alpha} U_\alpha n_{i\alpha\uparrow} n_{i\alpha\downarrow}, \quad (3)$$

$$\mathcal{H}_V = \sum_{\langle i\alpha; j\beta \rangle} \sum_{\sigma\sigma'} V_{i\alpha; j\beta} n_{i\alpha\sigma} n_{j\beta\sigma'}, \quad (4)$$

where i, j ($\in 1, \dots, N_L$) denote the lattice points of the 2D square lattice, and α, β ($\in 1, 2$) specify molecules in the unit cell. $c_{i\alpha\sigma}^\dagger$ ($c_{i\alpha\sigma}$) is the creation (annihilation) operator for an electron with spin σ ($= \uparrow, \downarrow$). $\langle i\alpha; j\beta \rangle$ represents a bond pair between the nearest neighbor sites. $t_{i\alpha; j\beta}$ denotes the transfer energy between sites (i, α) and (j, β) . \mathcal{H}_U and \mathcal{H}_V denote repulsive interactions where U_α and $V_{\alpha\beta}$ are the coupling for the on-site and those for the nearest neighbor sites, respectively. By using the Fourier transformation,

$$c_{i\alpha\sigma} = \frac{1}{\sqrt{N_L}} \sum_{\mathbf{k}} e^{i\mathbf{k}\cdot\mathbf{r}_i} c_{\mathbf{k}, \alpha, \sigma}, \quad (5)$$

eq. (1) is rewritten as

$$\begin{aligned} \mathcal{H} = & \sum_{\mathbf{k}\alpha\beta\sigma} (\varepsilon_{\alpha\beta}(\mathbf{k}) c_{\mathbf{k}\alpha\sigma}^\dagger c_{\mathbf{k}\beta\sigma} + \text{H.c.}) \\ & + \frac{1}{N_L} \sum_{\mathbf{k}\mathbf{k}'\mathbf{q}\alpha} U_\alpha c_{\mathbf{k}+\mathbf{q}, \alpha, \uparrow}^\dagger c_{\mathbf{k}, \alpha, \uparrow} c_{\mathbf{k}'-\mathbf{q}, \alpha, \downarrow}^\dagger c_{\mathbf{k}', \alpha, \downarrow} \\ & + \frac{1}{2N_L} \sum_{\mathbf{k}\mathbf{k}'\mathbf{q}\alpha\beta\sigma\sigma'} V_{\alpha\beta}(\mathbf{q}) c_{\mathbf{k}+\mathbf{q}, \alpha, \sigma}^\dagger c_{\mathbf{k}, \alpha, \sigma} c_{\mathbf{k}'-\mathbf{q}, \beta, \sigma'}^\dagger c_{\mathbf{k}', \beta, \sigma'} \end{aligned} \quad (6)$$

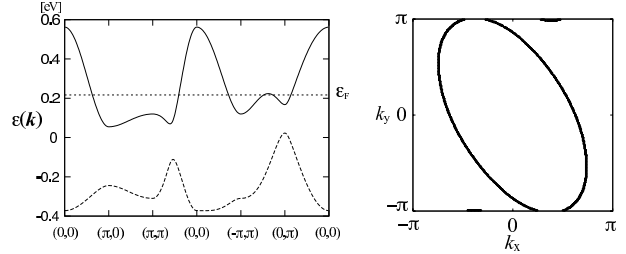


Fig. 2. Energy band spectra ξ_1 and ξ_2 of eq. (13) and the Fermi surface.

where the parameters in eq. (6) are taken as, $\varepsilon_{11} = \varepsilon_{22}$, $\varepsilon_{12} = \varepsilon_{21}^*$, $V_{11} = V_{22}$, $V_{12} = V_{21}^*$. Then the transfer energies are

$$\varepsilon_{11}(\mathbf{k}) = 2t_p \cos k_x, \quad (7)$$

$$\varepsilon_{12}(\mathbf{k}) = t_{r1} e^{-ik_y} + t_{r2} + t_{q1} e^{ik_x} + t_{q2} e^{-i(k_x+k_y)} \quad (8)$$

The long range Coulomb interactions become

$$V_{11}(\mathbf{q}) = 2V_p \cos q_x, \quad (9)$$

$$V_{12}(\mathbf{q}) = V_{r1} e^{-iq_y} + V_{r2} + V_{q1} e^{iq_x} + V_{q2} e^{-i(q_x+q_y)} \quad (10)$$

Applying the mean field approximation, the Hamiltonian is given by

$$\mathcal{H}_{\text{MF}} = \sum_{\mathbf{k}\alpha\beta\sigma} \tilde{\varepsilon}_{\alpha\beta\sigma}(\mathbf{k}) c_{\mathbf{k}\alpha\sigma}^\dagger c_{\mathbf{k}\beta\sigma} + \text{const.}, \quad (11)$$

$$\tilde{\varepsilon}_{\alpha\beta\sigma}(\mathbf{k}) = \varepsilon_{\alpha\beta}(\mathbf{k}) + \delta_{\alpha\beta} \left[U_\alpha \langle n_{\alpha\bar{\sigma}} \rangle + \sum_{\beta'\sigma'} V_{\alpha\beta'} \langle n_{\beta'\sigma'} \rangle \right], \quad (12)$$

where $\bar{\sigma}$ denotes the opposite spin of σ . In this approximation, we ignore the Fock term ($\langle c_{i\alpha}^\dagger c_{j\beta} \rangle \simeq 0$) and assume the uniform ground state: $\langle n_{\alpha\sigma} \rangle = 3/4$. The Hamiltonian is diagonalized as

$$E_{\text{MF}} = \sum_{\mathbf{k}\alpha\gamma\sigma} \xi_{\gamma\sigma}(\mathbf{k}) d_{\alpha\gamma\sigma}^*(\mathbf{k}) d_{\alpha\gamma\sigma}(\mathbf{k}), \quad (13)$$

where $\xi_1(\mathbf{k}) > \xi_2(\mathbf{k})$ (see Fig. 2). $d_{\alpha\gamma\sigma}(\mathbf{k})$ is the element of unitary matrix obtained by diagonalization of eq. (11). Then, $\langle n_{\alpha\sigma} \rangle$ is given as

$$\langle n_{\alpha\sigma} \rangle = \sum_{\gamma=1}^2 \frac{d_{\alpha\gamma\sigma}^*(\mathbf{k}) d_{\alpha\gamma\sigma}(\mathbf{k})}{\exp[(\xi_{\gamma\sigma}(\mathbf{k}) - \mu)/T] + 1}, \quad (14)$$

where μ is the chemical potential determined by the condition of 3/4-filling: $\frac{1}{2} \sum_{\alpha\sigma} \langle n_{\alpha\sigma} \rangle = \frac{3}{2}$.

2.2 Charge and spin susceptibilities

We define matrices of susceptibility as

$$(X_{\sigma\sigma'}(\mathbf{q}, i\omega_n))_{\alpha\beta} \equiv \frac{1}{N_L} \int_0^{1/T} d\tau e^{i\omega_n\tau} \langle n_{\alpha\sigma}(\mathbf{q})(\tau) n_{\beta\sigma'}(-\mathbf{q})(0) \rangle, \quad (15)$$

where ω_l is the Matsubara frequency for bosons.⁷ τ is the imaginary time. The density operator $n_{\alpha\sigma}(\mathbf{q})$ is given by

$$n_{\alpha\sigma}(\mathbf{q}) = \sum_{\mathbf{k}} c_{\mathbf{k}, \alpha, \sigma}^\dagger c_{\mathbf{k}+\mathbf{q}, \alpha, \sigma}. \quad (16)$$

The charge susceptibility \hat{X}^c and the spin susceptibility for the easy axis \hat{X}^s are given by

$$\hat{X}_{\alpha\beta}^c = \frac{1}{2}(\hat{X}_{\uparrow\uparrow} + \hat{X}_{\downarrow\uparrow} + \hat{X}_{\uparrow\downarrow} + \hat{X}_{\downarrow\downarrow})_{\alpha\beta}, \quad (17)$$

$$\hat{X}_{\alpha\beta}^s = \frac{1}{2}(\hat{X}_{\uparrow\uparrow} - \hat{X}_{\downarrow\uparrow} - \hat{X}_{\uparrow\downarrow} + \hat{X}_{\downarrow\downarrow})_{\alpha\beta}. \quad (18)$$

Applying the random phase approximation and ignoring the Fock term, we obtain

$$\begin{aligned} \hat{X}_{\sigma\sigma} &= [I + \hat{X}^{(0)}\hat{V}^{(1)} - \hat{X}^{(0)}\hat{V}^{(2)}(I + \hat{X}^{(0)}\hat{V}^{(1)})^{-1} \\ &\quad \times \hat{X}^{(0)}\hat{V}^{(2)}]^{-1}\hat{X}^{(0)}, \end{aligned} \quad (19)$$

$$\begin{aligned} \hat{X}_{\bar{\sigma}\sigma} &= -(I + \hat{X}^{(0)}\hat{V}^{(1)})^{-1}\hat{X}^{(0)}\hat{V}^{(2)}[I + \hat{X}^{(0)}\hat{V}^{(1)} \\ &\quad - \hat{X}^{(0)}\hat{V}^{(2)}(I + \hat{X}^{(0)}\hat{V}^{(1)})^{-1}\hat{X}^{(0)}\hat{V}^{(2)}]^{-1}\hat{X}^{(0)}. \end{aligned} \quad (20)$$

$\hat{V}^{(1)}$ and $\hat{V}^{(2)}$ are given by

$$\hat{V}^{(1)} = \hat{V} + \hat{U}, \quad \hat{V}^{(2)} = \hat{V} \quad (21)$$

where \hat{V} and \hat{U} are defined as

$$\hat{V} = \begin{pmatrix} V_{11}(\mathbf{q}) & V_{12}(\mathbf{q}) \\ V_{21}(\mathbf{q}) & V_{22}(\mathbf{q}) \end{pmatrix}, \quad \hat{U} = \begin{pmatrix} U & 0 \\ 0 & U \end{pmatrix}. \quad (22)$$

In this case, we treat mainly the nonmagnetic state, i.e., $X_{\uparrow\uparrow} = X_{\downarrow\downarrow}$, $X_{\uparrow\downarrow} = X_{\downarrow\uparrow}$. Then \hat{X}^c and \hat{X}^s are given by

$$\begin{aligned} \hat{X}^c &= \hat{X}_{\uparrow\uparrow} + \hat{X}_{\downarrow\downarrow} \\ &= (\hat{I} + \hat{X}^{(0)}(\hat{U} + 2\hat{V}))^{-1}\hat{X}^{(0)}, \end{aligned} \quad (23)$$

$$\begin{aligned} \hat{X}^s &= \hat{X}_{\uparrow\uparrow} - \hat{X}_{\downarrow\downarrow} \\ &= (\hat{I} - \hat{X}^{(0)}\hat{U})^{-1}\hat{X}^{(0)}, \end{aligned} \quad (24)$$

where \hat{X}^c and \hat{X}^s are hermitian matrices. The irreducible susceptibility $\hat{X}^{(0)}$ is

$$X_{\alpha\beta}^{(0)}(\mathbf{q}, i\omega_n) = -\frac{T}{N_L} \sum_{\mathbf{k}, n} G_{\alpha\beta}^{(0)}(\mathbf{k} + \mathbf{q}, i\omega_n + i\epsilon_n) G_{\beta\alpha}^{(0)}(\mathbf{k}, i\epsilon_n)$$

where ϵ_n denotes the Matsubara frequency for fermions. $G_{\alpha\beta}^{(0)}(\mathbf{k}, i\omega_n)$ is the single particle Green function given by

$$G_{\alpha\beta}^{(0)}(\mathbf{k}, i\epsilon_n) = \sum_{\gamma=1}^2 \frac{d_{\alpha\gamma}(\mathbf{k})d_{\beta\gamma}^*(\mathbf{k})}{i\epsilon_n - \xi_{\gamma}(\mathbf{k}) + \mu}, \quad (25)$$

where $\xi_{\gamma}(\mathbf{k})$ and $d_{\alpha\gamma}(\mathbf{k})$ are defined in eq. (13).

Now, we introduce the linear combinations of the density operators as

$$n_{\pm}(\mathbf{q}) = \frac{1}{\sqrt{2}}(n_1(\mathbf{q}) \pm n_2(\mathbf{q})). \quad (26)$$

Then replacing the original density operators in eq. (15), and taking account the symmetry in the unit cell, the corresponding charge ($\nu = c$) and spin ($\nu = s$) susceptibilities are given by

$$\begin{aligned} \hat{X}_{\pm}^{\nu} &= \frac{1}{2}(\hat{X}_{11}^{\nu} \pm \hat{X}_{21}^{\nu} \pm \hat{X}_{12}^{\nu} + \hat{X}_{22}^{\nu}) \\ &= \hat{X}_{11}^{\nu} \pm \text{Re } \hat{X}_{12}^{\nu}. \end{aligned} \quad (27)$$

The stability of the CO states in the present analysis (see Fig. 1 (b), (c)) is given by divergence of \hat{X}_{-}^c .

2.3 Pairing interactions and Eliashberg equations

The superconducting transition point is determined by the Eliashberg equation. The linearized Eliashberg equation for the singlet SC state is given by

$$\begin{aligned} \lambda_S \Sigma_{\alpha\sigma;\beta\bar{\sigma}}^a(\mathbf{k}) &= -\frac{1}{N_L} \sum_{\mathbf{k}', n', \alpha', \beta'} P_{\alpha\sigma;\beta\bar{\sigma}}^S(\mathbf{k} - \mathbf{k}') \\ &\quad \times G_{\alpha\alpha'}^{(0)}(\mathbf{k}', i\epsilon_{n'}) G_{\beta\beta'}^{(0)}(-\mathbf{k}', -i\epsilon_{n'}) \Sigma_{\alpha'\sigma;\beta'\bar{\sigma}}^a(\mathbf{k}'), \end{aligned} \quad (28)$$

with the paring interaction,

$$\hat{P}^S = \hat{U} + \hat{V} + \frac{3}{2}\hat{U}\hat{X}^s\hat{U} - \frac{1}{2}(\hat{U} + 2\hat{V})\hat{X}^c(\hat{U} + 2\hat{V}), \quad (29)$$

where \hat{X}^c and \hat{X}^s are the susceptibility matrices given in eqs.(23) and (24). In eq. (28), $\Sigma_{\alpha\sigma;\beta\bar{\sigma}}^a(\mathbf{k})$ is the anomalous self-energy with the space inversion symmetry $\Sigma_{\alpha\sigma;\beta\bar{\sigma}}^a(\mathbf{k}) = \Sigma_{\beta\bar{\sigma};\alpha\bar{\sigma}}^a(-\mathbf{k})$. Here we neglect the dependence of the Matsubara frequency in $\Sigma_{\alpha\sigma;\beta\bar{\sigma}}^a(\mathbf{k})$, since such a treatment is valid for the weak coupling case.¹¹ In eq. (28), $\lambda_S = 1$ corresponds to the superconducting transition point.

Similarly, the linearized Eliashberg equation for the triplet SC state is obtained as

$$\begin{aligned} \lambda_T \Sigma_{\alpha\sigma;\beta\sigma}^a(\mathbf{k}) &= -\frac{1}{N_L} \sum_{\mathbf{k}', n', \alpha', \beta'} P_{\alpha\sigma;\beta\sigma}^T(\mathbf{k} - \mathbf{k}') \\ &\quad \times G_{\alpha\alpha'}^{(0)}(\mathbf{k}', i\epsilon_{n'}) G_{\beta\beta'}^{(0)}(-\mathbf{k}', -i\epsilon_{n'}) \Sigma_{\alpha'\sigma;\beta'\sigma}^a(\mathbf{k}'), \end{aligned} \quad (30)$$

with the paring interaction,

$$\hat{P}^T = \hat{V} - \frac{1}{2}\hat{U}\hat{X}^s\hat{U} - \frac{1}{2}(\hat{U} + 2\hat{V})\hat{X}^c(\hat{U} + 2\hat{V}). \quad (31)$$

In order to confirm the relevant part of the effective interaction for the singlet state, we divide the paring interaction into the following two parts,

$$\hat{P}^c = \hat{V} - \frac{1}{2}(\hat{U} + 2\hat{V})\hat{X}^c(\hat{U} + 2\hat{V}), \quad (32)$$

$$\hat{P}^s = \hat{U} + \frac{3}{2}\hat{U}\hat{X}^s\hat{U}. \quad (33)$$

3. Numerical Results

In the present model, there are a lot of parameters, so that we select set of parameters in the following way: First, we fix the values of the transfer integrals from the results of the extended Hückel method: $t_{r1} = -0.0824$, $t_{r2} = -0.226$, $t_p = 0.0475$, $t_{q1} = -0.0438$, $t_{q2} = -0.115$ [eV].¹³ In this case, we do not consider explicit pressure dependence of the parameters. Next, we determine the value of the on-site Coulomb energy U so that the ground state becomes nonmagnetic. Then we determine the value of the nearest neighbor interactions V , so that the checkerboard type CO state is stabilized. We use the unit for the energies as [eV]. Finally, we determine the phase diagram of this model.

3.1 Nonmagnetic state

To obtain the phase diagram in the (U, T) plane (Fig. 3(a)), we calculate X_{+}^s which is larger than X_{-}^s . Fig. 3(b) shows the momentum dependence of the spin susceptibilities X_{+}^s , at $T = 0.1$. When the system is dimerized, the exchange coupling $J = \frac{4t^2}{U}$ becomes

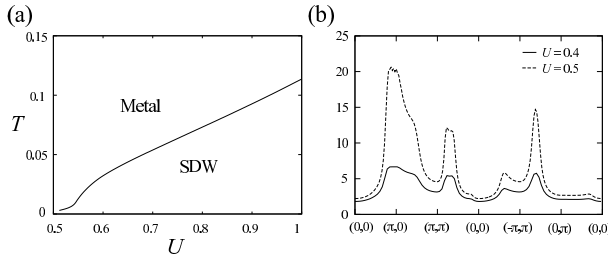


Fig. 3. (a) Phase diagram on the (U, T) plane. The solid line corresponds to the phase boundary between the metallic and the SDW states. (b) Spin susceptibilities $X_+^s(\mathbf{q})$ for $U = 0.4$ and 0.5 at $T = 0.01$.

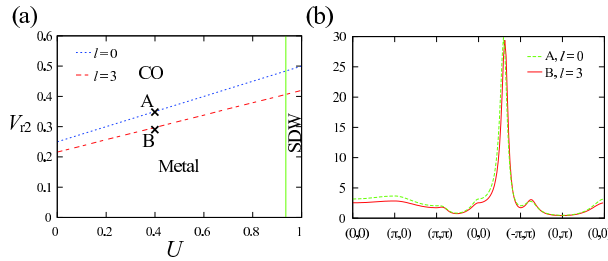


Fig. 4. (a) Phase diagram on (U, V_{r2}) plane at $T = 0.1$. The dashed and the solid lines corresponds to the CO and the SDW instabilities, respectively. (b) Charge susceptibilities $X_-^c(\mathbf{q})$ for $(V_{r2}, l) = (0.35, 0), (0.294, 3)$ at $T = 0.1, U = 0.4$.

$J_x > J_{xy} > J_y$, where $|t_x| = |t_p - t_{q1}/2| = 0.069 > |t_{xy}| = |t_{q2}|/2 = 0.056 > |t_y| = |t_{r1}/2| = 0.0412$.² As the result, X_+^s becomes large at $(\pi, 0)$. In this case, β -(DMeET)₂PF₆ is nonmagnetic. Therefore, the on-site Coulomb interaction U are fixed at 0.4 [eV] where the spin density wave (SDW) does not appear, in the following calculation.

3.2 Charge ordered states

We investigate the combination of the nearest neighbor Coulomb interactions V , where the checkerboard type charge order is stabilized. First, we examine the charge order patterns by using the point charge approximation: $V_i \propto \frac{1}{r_i}$. Fig. 4(a) shows the phase diagram on the (U, V_{r2}) plane at $T = 0.1$. \hat{X}_-^c becomes larger in the intermediate region between $(0, 0)$ and (π, π) as shown in Fig. 4(b), therefore we find that this result does not accord with the experimental fact. Taking account of the effective molecule size l , the coulomb interaction in the dimer is given as $V_{r2} \propto (r_{r2}^2 + l^2)^{-1/2}$. It is reported that $l \approx 3$ Å is reasonable for the ET salt.¹⁹ Therefore we fix l at 3 Å and apply the point charge approximation for the other V s. Fig. 4(a) shows (U, V_{r2}) -phase diagram for $T = 0.1$. In the case of $l = 3$ Å, the CO instability occurs in the smaller V_{r2} than that of $l = 0$ Å. This indicates that the charge fluctuation becomes larger by taking account of the molecule size, because the difference between V_{r2} and another V is smaller. However, the critical point of $X_-^c(\mathbf{q})$ does not change and we cannot obtain the checkerboard type charge ordering.

In order to stabilize the checkerboard type CO

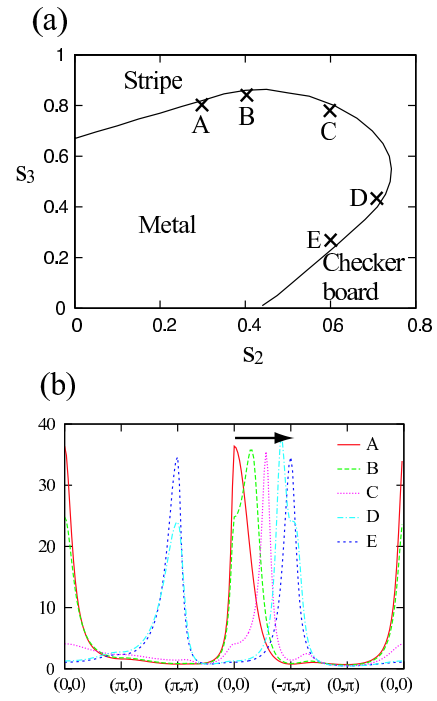


Fig. 5. (a) Phase diagram on (s_2, s_3) plane at $T = 0.1, U = 0.4, V_{r2} = 0.8U$. The solid line corresponds to the CO instability. (b) Charge susceptibilities $X_-^c(\mathbf{q})$ for $(s_2, s_3) = A(0.3, 0.8), B(0.4, 0.84), C(0.6, 0.25), D(0.7, 0.41)$ and $E(0.6, 0.78)$ at $T = 0.1, U = 0.4, V_{r2} = 0.8U$. The arrow shows the shift of the peak of $X_-^c(\mathbf{q})$ from $(0, 0)$ to (π, π)

state, it is suitable to satisfy the following condition: $(V_{r2}, V_p, V_{q2}) > (V_{r1}, V_{q1})$. For simplicity, we assume only two sets of nearest neighbor interactions $V_1 (= V_p = V_{q2})$ and $V_2 (= V_{r1} = V_{q1})$. As shown in Fig. 1(b), V_1 is the interaction for the occurring disproportion of the charge density in the unit cell: $n_{i1} \neq n_{i2}$. V_2 is the interaction to favor the uniform charge density in the unit cell: $n_{i1} = n_{i2}$. We set $V_{r2} = s_1 \times U$, $V_1 = V_p = V_{q2} = s_2 \times V_{r2}$, $V_2 = V_{r1} = V_{q1} = s_3 \times V_{r2}$. For nonmagnetic states, we fix U at 0.4 eV and $V_{r2} = 0.8 \times U$ as shown in Fig. 3(a).

Fig. 5 shows the phase diagram on the (s_2, s_3) plane. As shown in Fig. 3(b), a peak of X_-^c appears at $(0, 0)$ in the stripe type CO phase (Fig. 1(c)), and (π, π) in the checkerboard type CO phase (Fig. 1(b)). The wave number for the peak of X_-^c changes continuously in the intermediate region between the stripe and the checkerboard type CO regimes. In the parameter region of the point charge approximation, s_2 is nearly equal to s_3 , but s_2 should be sufficiently larger than s_3 to realize the checkerboard type CO state. When we take account of the correspondence with the real material, it is suitable that the difference between s_2 and s_3 is small. Therefore, we set $s_3 = 0.3$.

Next, we examine the CO state by varying the temperature. The obtained phase diagram is shown in Fig. 6(a). There is a reentrant charge order transition as a function of temperature similar to the result of the extended Hubbard model in the 2D square lattice.²⁰ We consider that this reentrant behavior is due to the competition

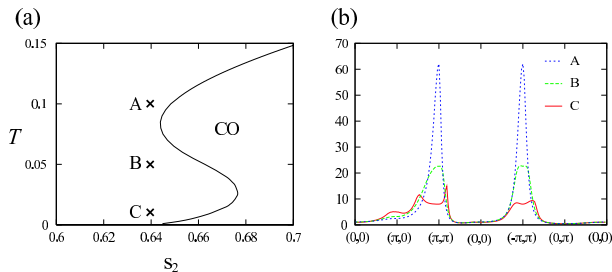


Fig. 6. (a) Phase diagram for the CO state on the (s_2, T) plane at $U = 0.4, V_{r2} = 0.8U, V_2 = 0.3V_{r2}$. The solid line corresponds to the CO instability. (b) Charge susceptibilities $X_c^c(\mathbf{q})$ for $T = 0.1, 0.05$ and 0.01 at $U = 0.4, V_{r2} = 0.8U, V_1 = 0.64V_{r2}, V_2 = 0.3V_{r2}$.

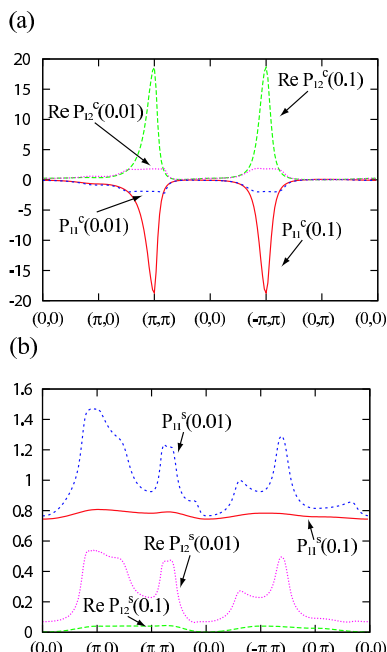


Fig. 7. Momentum dependence of the pairing interactions for the (a) charge [eq. (32)] and the (b) spin parts [eq. (33)], $P_{\alpha\beta}^{c(s)}(T)$, at $U = 0.4, V_{r2} = 0.8U$ and $V_2 = 0.3V_{r2}$. We set $s_2 = 0.64$ at $T = 0.1$ and $s_2 = 0.613$ at $T = 0.01$, respectively.

between the effect of $V(\mathbf{q})$ and $X^{(0)}(\mathbf{q})$: At high temperatures, the peak of X_c^c is near (π, π) . This originates from the momentum dependence of $V(\mathbf{q})$. With decreasing the temperature, the momentum dependence of $X^{(0)}(\mathbf{q})$ becomes large. Thus the peak of $X_c^c(\mathbf{q})$ changes from (π, π) as shown in Fig. 6 (b).

3.3 Pairing interactions and superconducting states

First, we examine the effect of \hat{P}^c . Fig. 7(a) shows the momentum dependence of \hat{P}^c . At $(s_2, T) = (0.64, 0.1)$, \hat{P}_{11}^c shows a negative peak at (π, π) , whereas \hat{P}_{12}^c shows a positive peak. This result is consistent with the appearance of the checkerboard-type charge ordering. The effective repulsive interaction is caused by the larger Coulomb interaction than V_2 : V_{r2} and V_1 . On the other hand, the effective attractive interaction arises by other Coulomb interactions V_2 . At $(s_2, T) = (0.64, 0.01)$, the peak of \hat{P}^c is suppressed and changes from (π, π) . We think it originates from the reentrant behavior of the CO.

The momentum dependence of P^s is determined by that of $\hat{X}^{(0)}$, because U does not depend on the momentum. As shown in Fig. 7(b), the momentum dependence of P^s increases with lowering the temperature. It is notable that \hat{P}^c is much larger than \hat{P}^s at $T = 0.1$ meaning that the SC state originates from the charge fluctuation. However, at $T = 0.01$, both \hat{P}^c and \hat{P}^s are the same order. Therefore we expect that the SC state in this region is caused by both the charge and the spin fluctuations.

In order to estimate the onset temperature for the SC states, we evaluate the linearized Eliashberg equations eqs. (28), (30). Then we obtain the phase diagram on the (s_2, T) plane as shown in Fig. 8. From Fig. 8 the singlet SC state competes with the triplet SC state for $0.05 < T$, but the singlet SC transition occurs first for $T < 0.05$. This means that an incommensurate CO phase is developed as lowering the temperature.

As shown in Figs. 9 and 10, the anomalous self-energy of the singlet SC state strongly depends on the temperature. For the singlet SC state at $T = 0.1$, $\text{Re } \Sigma_{12}$ is larger than Σ_{11} . This indicates that $\text{Re } \Sigma_{12}$ contributes mainly to the SC state at $T = 0.1$. On the other hand, $\text{Re } \Sigma_{12}$ is the same order of Σ_{11} . This indicates that both Σ_{11} and $\text{Re } \Sigma_{12}$ contribute to the SC state at $T = 0.01$. As mentioned above, the spin fluctuation increases with lowering the temperature (Fig. 7) and P^s is the same order of P^c at $T = 0.01$. The pairing interactions do not have a special peak, since the anomalous self-energies are broad.

The anomalous self-energy of the triplet SC does not depend much on the temperature as shown in Fig. 11. $\text{Re } P_{12}^s$ is smaller than P_{11}^s . It follows from eq. (31) that the total pairing interaction of the triplet SC state is given by $\hat{P}^T = \hat{P}^c - \frac{1}{3}(\hat{P}^s - \hat{U})$. This indicates that the triplet SC state is not strongly effected by the spin fluctuation than the singlet SC state. Therefore, we consider that the triplet SC state is mainly induced by the charge fluctuation. It is reasonable that the triplet SC state appears near the CO state.

The present system has only the space inversion symmetry. Therefore, we can classify the symmetry of the SC gaps as parity even and odd for the singlet and the triplet SC states, respectively. In order to determine the symmetry of the order parameters in more detail, we should calculate the quasi particle bands and count the numbers of crossing points at the Fermi surface. In the present linearized Eliashberg equations, however, the amplitude of the anomalous energies can be chosen arbitrary, so that we can not calculate the quasi particle bands.

4. Summary and Discussion

We have theoretically examined the CO and the SC states of β -(DMeET)₂PF₆. We have analyzed the extended Hubbard model including the nearest Coulomb interactions in the weakly dimerized lattice. Applying the RPA, we choose the suitable parameters realizing the checkerboard type CO state under the nonmagnetic state. The CO phase shows reentrant behavior as a function of the temperature. We consider that this behavior originates from the competition between the wave vec-

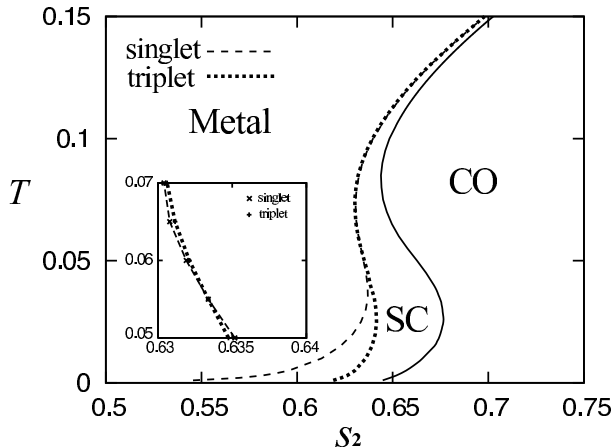


Fig. 8. Phase diagram on (s_2, T) plane at $U = 0.4, V_{r2} = 0.8U, V_2 = 0.3V_{r2}$. The solid line corresponds to the CO instability. Note that the superconducting (SC) region is overestimated in the present analysis for the high-temperature region. The inset shows the detail close to $T = 0.06$ where the triplet SC state competes with the singlet SC state.

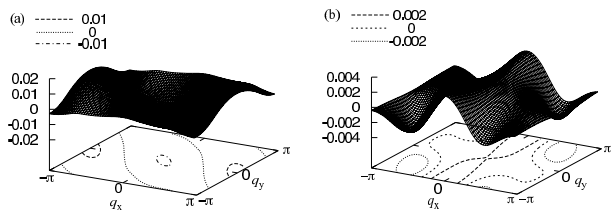


Fig. 9. The momentum dependence of the element of anomalous self-energy matrix Σ_{11} of the singlet SC state for (a) $T=0.01, s_2=0.613$ and (b) $T=0.1, s_2=0.64$.

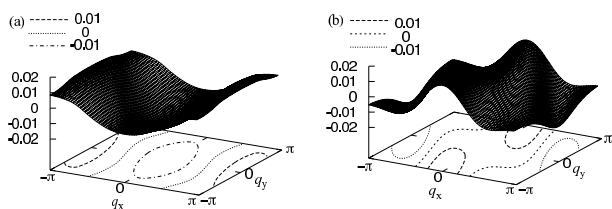


Fig. 10. The momentum dependence of the element of anomalous self-energy matrix $\text{Re}\Sigma_{12}$ of the singlet SC state for (a) $T=0.01, s_2=0.613$ and (b) $T=0.1, s_2=0.64$.

tor dependence of V and the nesting effect of the charge susceptibility.

Using the pairing interactions induced by the charge and spin fluctuations in terms of the RPA, we have estimated the onset temperature of the SC state near the CO instability by the linearized Eliashberg equations. The triplet SC state is stabilized around the region of the CO instability which originates from the wave vector dependence of $V(\mathbf{q})$. On the other hand, the singlet SC state is stabilized near the region of the CO instability which originates from the nesting vector of the Fermi surface.

The determination of parameters of the present model has been done to realize the checkerboard type CO state

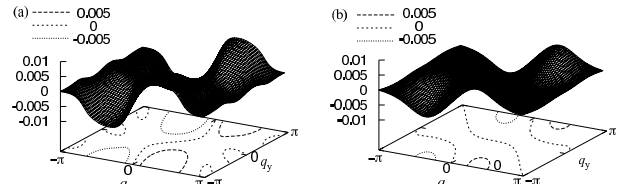


Fig. 11. The momentum dependence of the element of anomalous self-energy matrix Σ_{11} of the triplet SC state for (a) $T=0.01, s_2=0.636$ and (b) $T=0.1, s_2=0.64$.

under the nonmagnetic state, comparing with the experimental result. However, values of these parameters are much different from those expected by the point charge approximation, even taking account of the effective molecule size. This suggests the possibility of effects of the electron-phonon interaction due to the lattice distortion.

In this paper, we have assumed that the CO state is an insulating state. There is a possibility, however, that the CO state is a metallic state due to existence of the hole and the electron pocket in the Fermi surface, and a SC state coexists with the CO state in this case. This scenario was asserted to explain the superconductivity of α -(ET)₂I₃ salt under uniaxial pressure.^{7,8} Actually, the temperature and the pressure dependence of the resistivity in certain parameter regions seem to behave similarly in these two systems.^{13,21} In this case, the phase diagram of Fig. 8 may be modified so that a different type of SC state appears in the CO region.

5. Acknowledgements

The authors thank Y. Suzumura and A. Kobayashi for discussion and many helpful suggestions. We acknowledge T. Kato for helpful comments on the mean field calculation, and Y. Tanaka for discussion about the numerical analysis of the linearized Eliashberg equations. We are also grateful to H. Fukuyama and C. Ishii for useful comments. One of the authors (M. N.) is partly supported by the Grant-in-Aid for scientific research of the Ministry of Education, Science and Culture of Japan.

- 1) T. Ishiguro, K. Yamaji and G. Saito: *Organic Superconductors* (Springer-Verlag, Berlin, 1998) 2nd ed.
- 2) H. Seo, C. Hotta and H. Fukuyama: *Chem. Rev.* **104** (2004) 5005, and references therein.
- 3) H. Kino and H. Kontani: *J. Phys. Soc. Jpn.* **67** (1998) 3691.
- 4) H. Kondo and T. Moriya: *J. Phys. Soc. Jpn.* **67** (1998) 3695.
- 5) M. Vojita and E. Dagotto: *Phys. Rev. B* **59** (1999) R713.
- 6) T. Jujo, S. Koikegami and K. Yamada: *J. Phys. Soc. Jpn.* **68** (1999) 1331.
- 7) A. Kobayashi, S. Katayama, K. Noguchi and Y. Suzumura: *J. Phys. Soc. Jpn.* **73** (2004) 3135.
- 8) A. Kobayashi, S. Katayama and Y. Suzumura: *J. Phys. Soc. Jpn.* **74** (2005) 2897.
- 9) H. Seo: *J. Phys. Soc. Jpn.* **69** (2000) 805.
- 10) M. Kaneko and M. Ogata: *J. Phys. Soc. Jpn.* **75** (2006) 14710.
- 11) Y. Tanaka, Y. Yanase and M. Ogata: *J. Phys. Soc. Jpn.* **73** (2004) 2053, and references therein.
- 12) S. Kimura, H. Suzuki, T. Maejima, H. Mori, J. Yamaura, T. Kakiuchi, H. Sawa and H. Moriyama: *J. Am. Chem. Soc.* **128**

(2006) 1456.

- 13) S. Kimura, T. Maejima, H. Suzuki, R. Chiba, H. Mori, T. Kawamoto, T. Mori, H. Moriyama, Y. Nishimoto and K. Kajita: *Chem. Commun.* (2004) 2454.
- 14) H. Mori: *J. Phys. Soc. Jpn.* **75** (2006) 051003.
- 15) D. Jaccard, K. Behnia and J. Sierro: *Phys. Lett. A* **163** (1992) 475.
- 16) N. D. Mathur, F. M. Grosche, S. R. Julian, I. R. Walker, D. M. Freye, R. K. W. Haselwimmer and G. G. Lonzarich: *Nature* **394** (1998) 39.
- 17) S. S. Saxena, P. Agarwal, K. Ahilan, F. M. Grosche, R. K. W. Haselwimmer, M. J. Steiner, E. Pugh, I. R. Walker, S. R. Julian, P. Monthoux, G. G. Lonzarich, A. Huxley, I. Sheikin, D. Braithwaite and J. Flouquet: *Nature* **406** (2000) 587.
- 18) T. Yamauchi, Y. Ueda and N. Mori: *Phys. Rev. Lett.* **89** (2002) 057002.
- 19) M. Tamura and R. Kato: *J. Phys. Soc. Jpn.* **73** (2004) 3108.
- 20) A. Kobayashi, Y. Tanaka, M. Ogata and Y. Suzumura: *J. Phys. Soc. Jpn.* **73** (2004) 1115.
- 21) N. Tajima, A. E. Tajima, M. Tamura, Y. Nishio and K. Kajita: *J. Phys. Soc. Jpn.* **71** (2002) 1832.